Model Organisms: New Insights: Into Ion Channel and Transporter Function. Caenorhabditis elegans ClC-type chloride channels: novel variants and functional expression

Keith Nehrke, Ted Begenisich, Jodi Pilato and James E. Melvin

You might find this additional information useful...

This article cites 43 articles, 14 of which you can access free at:
http://ajpcell.physiology.org/cgi/content/full/279/6/C2052#BIBL

This article has been cited by 8 other HighWire hosted articles, the first 5 are:

CLC-0 and CFTR: Chloride Channels Evolved From Transporters
T.-Y. Chen and T.-C. Hwang
Physiol Rev, April 1, 2008; 88 (2): 351-387.
[Abstract] [Full Text] [PDF]

Evolutionarily conserved WNK and Ste20 kinases are essential for acute volume recovery and survival after hypertonic shrinkage in Caenorhabditis elegans
K. P. Choe and K. Strange
Am J Physiol Cell Physiol, September 1, 2007; 293 (3): C915-C927.
[Abstract] [Full Text] [PDF]

Altered gating and regulation of a carboxy-terminal ClC channel mutant expressed in the Caenorhabditis elegans oocyte
J. Denton, K. Nehrke, X. Yin, A. M. Beld and K. Strange
Am J Physiol Cell Physiol, April 1, 2006; 290 (4): C1109-C1118.
[Abstract] [Full Text] [PDF]

GCK-3, a Newly Identified Ste20 Kinase, Binds To and Regulates the Activity of a Cell Cycle-dependent ClC Anion Channel
J. Denton, K. Nehrke, X. Yin, R. Morrison and K. Strange
J. Gen. Physiol., January 31, 2005; 125 (2): 113-125.
[Abstract] [Full Text] [PDF]

From Genes to Integrative Physiology: Ion Channel and Transporter Biology in Caenorhabditis elegans
K. Strange
Physiol Rev, April 1, 2003; 83 (2): 377-415.
[Abstract] [Full Text] [PDF]

Medline items on this article's topics can be found at http://highwire.stanford.edu/lists/artbytopic.dtl
on the following topics:

Physiology .. Chloride Channel
Physiology .. Ion Channels
Biochemistry .. Complementary DNA
Entomology .. Nematodes
Genetics .. Transgenic Animals
Physiology .. Nematoda

Updated information and services including high-resolution figures, can be found at:
http://ajpcell.physiology.org/cgi/content/full/279/6/C2052

Additional material and information about *AJP - Cell Physiology* can be found at:
http://www.the-aps.org/publications/ajpcell

This information is current as of July 8, 2010 .

special topics

Model Organisms: New Insights Into Ion Channel and Transporter Function. *Caenorhabditis elegans* ClC-type chloride channels: novel variants and functional expression

KEITH NEHRKE,[1] TED BEGENISICH,[2] JODI PILATO,[1] AND JAMES E. MELVIN[1,3]
[1]*Center for Oral Biology, Aab Institute of Biomedical Sciences,* [2]*Department of Pharmacology and Physiology,* and [3]*Eastman Department of Dentistry, University of Rochester Medical Center, Rochester, New York 14642*

Nehrke, Keith, Ted Begenisich, Jodi Pilato, and James E. Melvin. *Caenorhabditis elegans* ClC-type chloride channels: novel variants and functional expression. *Am J Physiol Cell Physiol* 279: C2052–C2066, 2000.—Six ClC-type chloride channel genes have been identified in *Caenorhabditis elegans*, termed *clh-1* through *clh-6*. cDNA sequences from these genes suggest that *clh-2*, *clh-3*, and *clh-4* may code for multiple channel variants, bringing the total to at least nine channel types in this nematode. Promoter-driven green fluorescent protein (GFP) expression in transgenic animals indicates that the protein CLH-5 is expressed ubiquitously, CLH-6 is expressed mainly in nonneuronal cells, and the remaining isoforms vary from those restricted to a single cell to those expressed in over a dozen cells of the nematode. In an Sf9 cell expression system, recombinant CLH-2b, CLH-4b, and CLH-5 did not form functional plasma membrane channels. In contrast, both CLH-1 and CLH-3b produced strong, inward-rectifying chloride currents similar to those arising from mammalian ClC2, but which operate over different voltage ranges. Our demonstration of multiple CLH protein variants and comparison of expression patterns among the *clh* gene family provides a framework, in combination with the electrical properties of the recombinant channels, to further examine the physiology and cell-specific role each isoform plays in this simple model system.

nematode; electrophysiology; transgenic; green fluorescent protein

EXPRESSION CLONING OF A VOLTAGE-GATED chloride channel gene from the electric organ of *Torpedo marmorata* provided the first member of the ClC family (16). Subsequently, at least nine genes have been shown to exist in mammals (1, 3, 8, 17, 35, 36, 38, 39). The function of these genes probably includes the control of electrical excitability, transepithelial transport, and the charge compensation necessary for the acidification of intracellular organelles (for review, see Ref. 15). In addition, ClC2 and ClC3 may play a role in cell volume regulation (41, 45). Evidence for the physiological significance of the ClCs includes mutations in the ClC1 muscle chloride channel that leads to myotonia (19, 34), in the ClCKb kidney-specific channel that leads to Bartter's syndrome [associated with severe renal wasting (32)], and in the ClC5 channel that leads to Dent's disease [associated with proteinuria and hypercalciuria (21)]. Furthermore, mice with targeted disruption of the *Clcnckl* gene display nephrogenic diabetes insipidus (24). ClC-like genes appear to be conserved from mammals to lower organisms including bacteria (23) and yeast (12).

Caenorhabditis elegans is a free-living soil nematode that feeds on bacteria and has a life cycle of ~3 days, although adults can live for several weeks after egg laying (for review, see Ref. 44). The adult hermaphrodite, which comprises the vast majority of the population, has 959 somatic nuclei, for which complete fate maps and lineage determinations exist. Juvenile worms develop into adults through a series of molts, resulting in four distinct larval stages (L1–L4). In addition to a complete wiring diagram being available for the *C. elegans* neuronal circuitry, the genome is completely sequenced.

The completion of the *C. elegans* genome sequencing project led to the prediction of a family of six voltage-gated chloride channel genes in nematodes. Recently,

---

the cDNA has been cloned for *clh-1* through *clh-5*, expression patterns have been determined for *clh-2*, *clh-3*, and *clh-4*, and recombinant CLH-3 has been characterized electrophysiologically by expression in *Xenopus* oocytes (31). In addition, it has been shown that disruption of the *clh-1* gene causes a defect in body width of the adult and that the *clh-1* gene product localizes to seam cells, a set of multinucleated cells that help to maintain the cuticle that encases the worm (29). Analysis of these cDNA sequences confirmed that the CLH proteins share many of the characteristics of mammalian ClC chloride channels (31): each contains two conserved cystathione β-synthase (CBS) domains of unknown function at the carboxy terminus and multiple membrane-spanning domains containing a conserved motif GKxGPxxH, which may act as a core structural element of the pore region (7).

In the present study, the cDNA sequence has been determined for all six *clh* isoforms, including *clh-6*. The sequences of the *clh-2, clh-3,* and *clh-4* clones appear to be different from those previously reported (31). The new variant proteins are named CLH-2b, CLH-3b, and CLH-4b. Some of these differences may be attributable to start site selection and/or alternative splicing patterns, and, in the case of the *clh-2* variants, suggests the use of entirely nonoverlapping promoters. In contrast to the previously described *clh-1* (31), which did not express functional channels, the variant we identified gave rise to voltage-dependent, inward-rectifying chloride currents. We also found that CLH-3b, despite significant differences in the amino acid sequences at both ends of the protein, generated currents that were generally similar to those described previously for CLH-3 (31). Promoter::GFP constructs were used to determine the expression patterns driven by the *clh-1, clh-2b, clh-3b, clh-4b, clh-5,* and *clh-6* genes. For *clh-2b*, we found that the expression pattern differed remarkably from that described for *clh-2* (31), suggesting that the two separate promoter elements may regulate expression of this gene in different cell types. We also detected strong expression from the *clh-1* and *clh-3b* promoters in cells not previously documented (29, 31). Furthermore, *clh-5* appears to be expressed ubiquitously, while *clh-6* appears to be expressed in most nonneuronal cells in the nematode.

EXPERIMENTAL PROCEDURES

cDNA cloning. Basic local alignment search tool homology searches of GenBank with mammalian ClC sequences yielded multiple expressed sequence tags and 6 genes spread over 10 genomic cosmid clones (*clh-1* on T27d12; *clh-2* on B0491 and C33b4; *clh-3* on E04f6 and F32a5; *clh-4* on T06f4 and R02e4; *clh-5* on C07h4 and T24h10; *clh-6* on R07b7). Isoform-specific probes were generated by RT-PCR and were targeted to sequences that lie near the 5′ end of the predicted coding regions (*clh-1*, nt 479−848; *clh-2*, nt 353−689; *clh-3*, nt 299−655; *clh-4*, nt 499−870; *clh-5*, nt 453−865; *clh-6*, nt 428−802). Probes were labeled by random priming using a Ready Prime DNA labeling kit (Life Technologies, Rockville, MD) and [^{32}P]dCTP. Nearly full-length coding regions for six of the ClC homologs were obtained by screening two *C. elegans* cDNA libraries: an oligo(dT)-primed cDNA library

and a random-primed cDNA library, λ-ACT-RB1 and λ-ACT-RB2, respectively (kindly provided by Dr. R. Barstead, University of Wisconsin-Madison). Seven hundred thousand phage of each library RB1 and RB2 were plated onto 24 × 24 cm Nunc plates and a lawn of LE392 *Escherichia coli* cells. The plates were plaque-lifted using Hybond-N membranes (Amersham Pharmacia Biotech, Piscataway, NJ), and the membranes were hybridized overnight at 42°C in 5× sodium chloride-sodium phosphate-EDTA, 50% formamide, 5× Denhardt solution, 0.1% SDS, and 100 μg/ml salmon sperm DNA, containing 5 × 10^5 cpm/ml of each ^{32}P-labeled denatured probe. Filters were washed three times for 20 min each in 2× SSC and 0.1% SDS at the following three temperatures: 42, 64, and 42°C. Initial screening was performed with a mixture of all six probes for isoforms *clh-1* through *clh-6*. Positive plaques were cored, dot-blotted on multiple Hybond-N membranes, and probed with individual isoform-specific probes, using the conditions above. Several clones that hybridized to each isoform-specific probe were isolated to homogeneity. Cre-lox excision of the pACT plasmid from each λ clone was accomplished by transduction into the *E. coli* strain RB4, which expresses the Cre recombinase. Quiagen quality plasmid DNA was prepared in the RB4 host and used directly for cycle DNA sequencing with ABI BigDye terminator mix and thermostable DNA polymerase on an MJResearch autosequencer. The reactions were run by the University of Rochester Core Nucleic Acids Facility. Both strands of all clones were completely sequenced.

Additional sequence information at the 5′ end of clones for *clh-1*, *clh-3b*, *clh-5*, and *clh-6* was derived from 5′ rapid amplification of cDNA ends using the SL1 trans-spliced leader sequence as an anchored primer and sequence corresponding to the 3′-most 22 nucleotides of the probes described above as an isoform-specific primer.

Electrophysiological analysis. Baculovirus expression constructs were generated for *clh-1*, *clh-2b*, *clh-3b*, *clh-4b*, and *clh-5* and for murine ClC2 by amplification of the entire coding region using *pfu* DNA polymerase and insertion as restriction-site tagged products, complete with an Sf9 insect cell translation initiation consensus sequence, into the pBlueBac4 vector (Invitrogen, Carlsbad, CA). Subsequently, portions of the PCR-derived coding sequence were replaced with that from the λ cDNA clones, and the inserts were completely sequenced. The PCR-generated clones were derived as follows: pBB-T27 contains the amplified coding region for *clh-1* inserted at *Nhe* I and *Hin*d III sites of pBlueBac4, pBB-C33 contains *clh-2b* inserted at *Nhe* I and *Hin*d III sites, pBB-E04 contains *clh-3b* inserted at *Nhe* I and *Bgl* II sites, pBB-T06 contains *clh-4b* inserted at *Nhe* I and *Bgl* II sites, pBB-C07 contains *clh-5* inserted at *Nhe* I and *Bam*H I sites, and pBB-ClC2 contains ClC2 inserted at *Bam*H I and *Eco*R I sites.

The final replacement expression vectors (in bold) were derived from those above as follows: an *Xho* I-*Mlu* I fragment of *clh-1* (nt 355−1957) in pBB-T27 was replaced with that from a lambda cDNA clone to generate **pB3-T27**. pBB-C33, the *clh-2b* expression clone, was sequenced completely and found to contain a single nucleotide deletion, which was repaired using a mutagene protocol with a wild-type oligonucleotide. The final construct, **pB3-C33**, was also sequenced completely. pB3-E04 contains a lambda-derived *Xba* I fragment of *clh-3b* (nt 669−2780), while **pB4-E04** further replaces a *Bst*B I-*Sal* I (nt 2875- MCS) fragment of pB3-E04 with a *Bst*B I-*Xho* I fragment from the lambda clone. **pB3-T06** contains a lambda-derived *Age* I-*Xho* I fragment of *clh-4b* (nt 940−2990). **pB3-ClC2** contains an *Nco* I fragment of mClC2 (nt 339−2080) from the vector m6B-6 (kindly pro-

vided by G. Borsani, Telethon Institute of Genetics and Medicine, Milan, Italy). Finally, **pBB-C07**, the first clone derived, was not substituted, but was sequenced completely to determine the extent of PCR-induced errors (of which there were several, all in the wobble position of the codon).

Using standard methods for the maintenance and transfection of Sf9 cells and the identification, amplification, and plaque assay of recombinant baculovirus (Invitrogen), the clones were expressed at a multiplicity of infection of 10 in Sf9 cells plated onto 5-mm glass coverslips. At 24 or 48 h postinfection, whole cell patch-clamp recordings were done at room temperature (20–22°C) using an Axopatch 1-D amplifier (Axon Instruments, Foster City, CA). The measured junction potentials for the solutions used were <1 mV, so no correction for these was applied. The holding potential was 0 mV. Data acquisition was performed using a 12-bit analog/digital converter controlled by a personal computer.

The standard external solution contained (in mM) 140 N-methyl-D-glucamine (NMDG) chloride, 2 $CaCl_2$, 2 $MgCl_2$, and 20 mM HEPES, pH 7.1 (with NMDG). The standard internal solution contained (in mM) 60 chloride, 60 glutamic acid, 120 (NMDG), 3 MgATP, 10 EGTA, and 10 HEPES, pH of 7.2 (with NMDG). Shortly after achieving whole cell mode with these solutions, an outward rectifying current developed in uninfected as well as infected Sf9 cells. This is likely the volume-sensitive organic osmolyte/anion channel (VSOAC; e.g., see Ref. 5). With these solutions, the activation of this current was transient: it disappeared within 10–15 min. The elimination of this current was accelerated if 30 mM mannitol was added to the standard external solution. Currents through the expressed channels CLH-1, CLH-3b, and ClC2 were the same with or without mannitol in the external solution. Since NMDG is impermeant to most channels, currents measured with these solutions are most likely carried by chloride ions.

As described in RESULTS, several different equations were fit to the data. These were done using the Simplex algorithm (4), either in our own implementation or that incorporated in the Origin software package (version 5.0; Microcal Software, Northampton, MA). When given, error limits for the fitted parameters are the estimated errors from the fitting routines.

To provide a quantitative measure of the voltage dependence of activation [$G(V_m)$], we converted the measured ionic current (I) to conductance

$$G(V_m) = \frac{I(V_m)}{V_m - V_{rev}} \qquad (1)$$

where V_m is the membrane potential and V_{rev} the current reversal potential. The rectifying nature of the expressed channels and the rapid deactivation kinetics of, for example, CLH-1, complicate the accurate measurement of the reversal potential. Both *C. elegans* channels and ClC2 had negative reversal potentials in the range −10 to −2 mV. In general, chloride channels are not particularly selective for anions and even glutamate is sparingly permeant in some channels [e.g., Arreola et al. (2)]. With our recording solutions, the reversal potential expected for a channel permeant to chloride and glutamate (0.1 the permeability of chloride) is −18 mV. Our more positive values likely reflect the difficulty of this measurement and the fact that any leak current will bias the measurements toward less negative potentials.

We fit a Boltzmann relation to the channel conductance

$$G(V_m) = \frac{A_1 - A_2}{1 + e^{(V_m - V_{1/2})/k}} + A_2 \qquad (2)$$

This equation allows a nonzero, likely leak conductance, A_2, at positive potentials where these channels are not activated. The voltage at which half the channels are activated is given by the $V_{1/2}$ parameter and the voltage sensitivity is governed by the k parameter.

Construction of clh::GFP promoter fusions and generation of transgenic animals. Nematodes (Bristol N2 strain) were cultured at 14°C or 18°C on NGM agar plates seeded with HB101 or OP50 bacteria from an overnight culture. GFP expression constructs for each *clh* gene consisted of ~4 kb of promoter sequence from upstream of the ATG translation initiation site, together with 10–12 nt downstream, cloned into expanded multiple cloning site vector pFH6(II) (courtesy of F. Hagen, University of Rochester, Rochester NY), which is a derivative of pPD 95.81 (courtesy of A. Fire, Carnegie Institute of Washington, Baltimore, MD). The inserts were PCR amplified from a genomic template. Both upstream and downstream oligonucleotides were tagged with unique restriction sites for cloning purposes. The downstream oligonucleotide was designed to be an imperfect match such that the genomic start site ATG would be mutated to a TTG in the final construct.

pJP72C07 contains the *clh-5* promoter and was amplified using oligonucleotides 5′-GCTCCTGTTGCTCAGCTGAA-GAAGACC-3′ and 5′-CGACCTGCTCGTTCCA**A**TTTCGGC-TGG-3′, with *Nhe* I and *Bam*H I tags, respectively (mutated residue from within the ATG codon is given in bold and underlined). Similarly, pJP72C33 (*clh-2*) used 5′-ACTACCG-AGCATCGCTGCAGGCTTGG-3′ and 5′-ACTTTTGCCAAT-GGATCCA**A**TGTTAAAGGAGTT-3′ with a *Pst* I tag on the upstream oligonucleotide and a *Bam*H I site internal (ORF nt +4) to the downstream primer; pJP72E04 (*clh-3*) used 5′-CAAATCAAGTGACGCAATCTGACTCGC-3′ and 5′-ACCA-ATACCCA**A**ACTTTTGGAATCCTCG-3′ with *Nhe* I and *Pst* I tags; pJP72R07 (*clh-6*) used 5′-GTAGATGGTGATCTGTT-TCTGGCTTGTG-3′ and 5′-CTGTTACGGGATGTCA**A**CTG-AAATGTTG-3′ with *Nhe* I and *Bam*H I tags; pJP72T06 (*clh-4*) used 5′-CCACATTGGTGGTGCTATGAATTCAGC-3′ and 5′-CGCACCGTTCA**A**ACGACAAAATTCAGGCG-3′ with *Nhe* I and *Bam*H I tags; pJP72T27 (*clh-1*) used 5′-CGG-AAATGGCCTTTATTTCCGCGCAC-3′ and 5′-GCGTCTTCC-A**A**CCTGATGTGCAGAATC-3′ with *Nhe* I and *Bam*H I tags.

GFP fusion construct and pRF4, which produces a *rol-6* roller phenotype (20), were mixed at 75 µg/ml each in injection buffer, then coinjected into the gonad of young adult Bristol N2 nematodes, as described in Ref. 26. After 4 days, rollers were picked from at least 10 injections to separate plates to look for germ line transmission. The nematodes were imaged on 2% agarose pads using a Nikon Eclipse E800 microscope equipped with a Nikon 60× oil objective under 100 W mercury illumination and a GFP or DAPI filter set, as appropriate. The images were captured using a Spot2 camera and analyzed in Adobe Photoshop (Adobe Systems, San Jose, CA). Due to the intensity of fluorescence from cells that are out of the plane-of-focus, many of the images that we present here are derived from mosaic animals.

RESULTS

The six ClC genes in C. elegans (clh-1 through clh-6) express at least nine distinct channels. Six ClC genes from *C. elegans*, termed *clh-1* through *clh-6*, have been previously described (29, 31). While the cDNA sequences reported here are similar in many ways to those identified previously, significant differences do occur in three of the five isoforms previously cloned, particularly in terms of start site selection and poten-

tial alternative splice patterns. The new mRNA variants described in the present report are denoted as *clh-2b, clh-3b*, and *clh-4b*. We also present the first cDNA sequence cloned from *clh-6*.

Figure 1*A* illustrates the genomic structure of the six nematode *clh* isoforms. For the three new variants that we have identified, the differences from the original clones are denoted schematically by a combination of
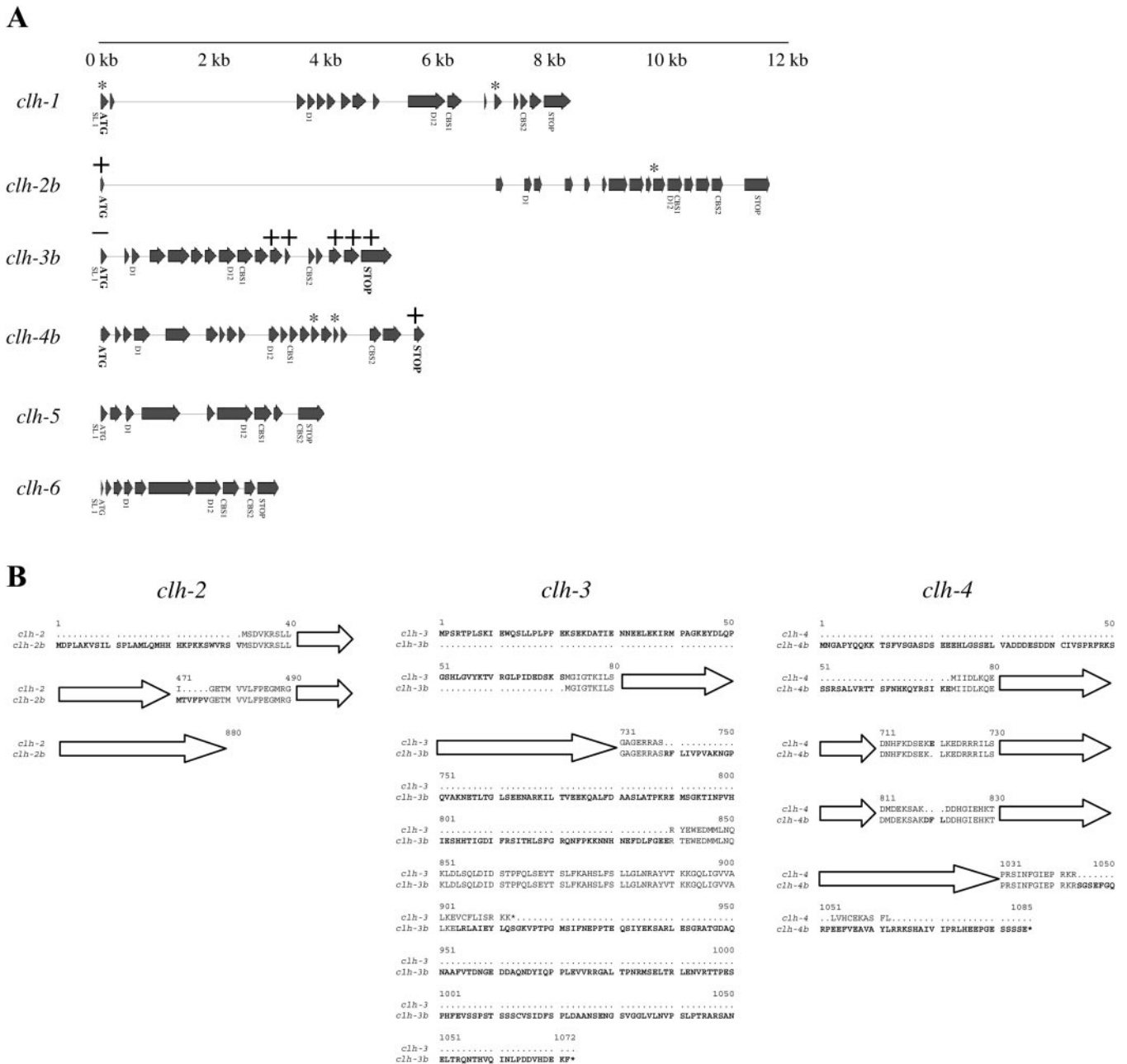

Fig. 1. *A*: gene organization of the *C. elegans clh* family. Arrows represent the coding regions of each gene and are drawn to scale with the intervening introns. The predicted translation start sites are indicated by an ATG and stop sites by a "stop." Transmembrane helices D1 and D12 are indicated to demonstrate the boundaries of the highly conserved transmembrane domain. Likewise, the start of CBS domains 1 and 2 are indicated. Those isoforms where an SL1 trans-spliced leader sequence was identified are denoted as such. The differences between *clh1, clh-2b*, *clh-3b*, and *clh-4b* and the originally identified isoforms (31) are displayed by using an asterisk (*) to denote a small insertion, deletion, or nucleotide change, a minus sign (−) to denote a missing exon(s), and a plus sign (+) to indicate a new exon(s). New start or stop sites are indicated by slightly larger, bold text. *B*: protein comparison of CLH-2, CLH-3, and CLH-4 variants. For each set of variants, a Clustal W algorithm [Thompson et al. (38a)] was used to align the two amino acid sequences. Regions where the sequences differ are presented in bold in the alignment, with the regions of similarity presented in either normal typeface or represented as arrows that connect the areas of divergence. In general, these differences represent alternative exons, translational start sites, or stop sites, as indicated above.

asterisks to indicate a small change, plus or minus signs to indicate new or missing exons, respectively, and boldface type at new ATG and translational stop sites. Amino acid sequence alignments suggest that the most divergent segments of CLH-2, CLH-3, and CLH-4 and CLH-2b, CLH-3b, and CLH-4b, respectively, lie at the amino and carboxy termini of the proteins, rather than in the core transmembrane domain, which is conserved even between isoforms (Fig. 1*B*).

In addition, there were several small differences between the cDNA sequence that we found for *clh-1* and a previously published sequence (31). A single nucleotide insertion that both we and Petalcorin et al. (29) predict occurs early in the transcript and results in the addition of 38 amino acids to the protein and may have functional consequences on the expression of CLH-1, because a previous attempt to express this protein was unsuccessful (31). This single nucleotide difference is not likely due to alternative splicing, and thus we do not refer to *clh-1* in terms of two variants.

Clh-2b contains an exon at the 5′ end that is not present in *clh-2*; an in-frame ATG adds 31 amino acids to the amino terminus of the predicted protein (indicated by a plus sign in Fig. 1*A*). Genomic sequence comparison indicates that the first intron is nearly 7 kb long (Fig. 1*A*). This was confirmed by amplification of a full-length clone from cDNA by RT-PCR. Moreover, we identified 15 additional nucleotides at the beginning of exon 11 in *clh-2b* (indicated by an asterisk), resulting in the addition of five amino acids within the putative transmembrane domain of this protein. Maturation of many nematode transcripts frequently includes the acquisition of an SL1 or SL2 trans-spliced leader (14, 40). While an SL1 splice site was found in *clh-2* (31), we were unable to identify an SL1 or SL2 leader for *clh-2b*. Amino acid alignments of *clh-2* and *clh-2b* are found in Fig. 1*B*.

Clh-3b lacks the first three exons of *clh-3* (indicated by a minus sign in Fig. 1) and contains a novel SL1 trans-spliced leader, resulting in use of an alternative translational start site and consequently the loss of 71 amino acids from the amino terminus. Multiple differences between *clh-3* and *clh-3b* were found within the carboxy terminus of the protein as well. Exons 11 and 12 of *clh-3b* are not present in *clh-3*, and *clh-3* ends after exon 14 of *clh-3b*, in what is predicted to be intron sequence (indicated by three plus signs in Fig. 1). This results in the use of an alternative stop site, as well as differences in the last 6 amino acids of the CBS2 domain, which occurs only 3 amino acids short of the stop codon in *clh-3* compared with 163 amino acids before the stop codon in *clh-3b*. A comparison of the results of these changes to the amino acid sequence of *clh-3* and *clh-3b* is shown in Fig. 1*B*.

We also found several differences between *clh-4* and *clh-4b*. The last exon in *clh-4* was found spliced to a new exon in *clh-4b* (exon 20, indicated by a plus sign in Fig. 1). This resulted in the substitution of the final 10 amino acids in *clh-4* with 42 amino acids from the new exon and the use of a new stop codon. There was also a 3-nt deletion at position 2155 of *clh-4b* between exons

13 and 14 and a 9-nt insertion at position 2453 between exons 15 and 16 (asterisks in Fig. 1), resulting in a net gain of two amino acids. Although the mRNA sequence at the 5′ end for *clh-4* and *clh-4b* is identical, the predicted amino acid sequence is not. This is due to the use of different predicted start codons. We suggest here that the *clh-4b* protein initiates at the first ATG in exon 1, near the predicted 5′ end of the mRNA. A previous report suggested that *clh-4* initiates at an internal ATG in exon 2, at 217 nucleotides from the 5′ end of the mRNA (31).

While the cDNA sequence that we identified for *clh-5* is identical to that described earlier (31), the cDNA sequence that we identified for *clh-6* has not previously been published. The intron-exon boundaries for *clh-6* are shown in Fig. 1. The coding regions for both *clh-5* and *clh-6* are shorter than the other isoforms and contain less introns. This is reflected in a lesser sequence homology compared with the other isoforms.

Expression of GFP from clh promoters in transgenic animals. Approximately 4 kb of promoter region from each *clh* gene, extending upstream from and including a mutated ATG-to-TTG initiator codon, was cloned as a transcriptional fusion with cDNA encoding a cytoplasmic form of GFP. These constructs were then injected with a *rol-6* marker plasmid that produces a roller phenotype into the Bristol N2 strain, and transgenic lines were established. Table 1 indicates where each of these constructs is expressed and incorporates expression data generated from several other groups as well (29, 31). Figure 2, *A* and *B*, is intended to provide orientation in the form of a general schematic of the nematode architecture, including the major organs, reproductive system, and neuron cell body locations.

Clh-1 promoter-driven expression has previously been localized to seam cells, which extend along the lateral sides of the body to form two seam syncytia in

Table 1. *Distribution of C. elegans chloride channels*

Promoter	GFP expression profile in *clh*∷GFP transgenic strains
clh-1	Seam cells and hypodermal cells of the head,* epithelial D-cell of the vulva, spermatheca, neurons in the head ganglia, and posterior intestinal cells
clh-2†	Ventral and dorsal nerve cords, neurons in the head and tail ganglia, nerve ring, and the pharyngeal-intestinal valve
clh-2b	Body wall muscle, posterior intestinal cells, and neurons in the head and tail ganglia
clh-3 and *clh-3b*‡	Excretory cell, vulva, hermaphrodite-specific neurons, enteric muscles, first four epithelial cells of intestine, and the uterus§
clh-4 and *clh-4b*‡	Excretory cell
clh-5	Ubiquitous
clh-6	Hypodermal cells, gut, and pharyngeal, body wall, vulval, intestinal, and enteric muscles, with much, much lower levels in several neurons; no expression was observed in seam cells or the excretory cell

GFP, green fluorescent protein. *As described both here and by Petalcorin et al. (29); †as described by Schriever et al. (31); ‡as described both here and by Schriever et al. (31); §uterine expression was noted only from the *clh-3b* construct.
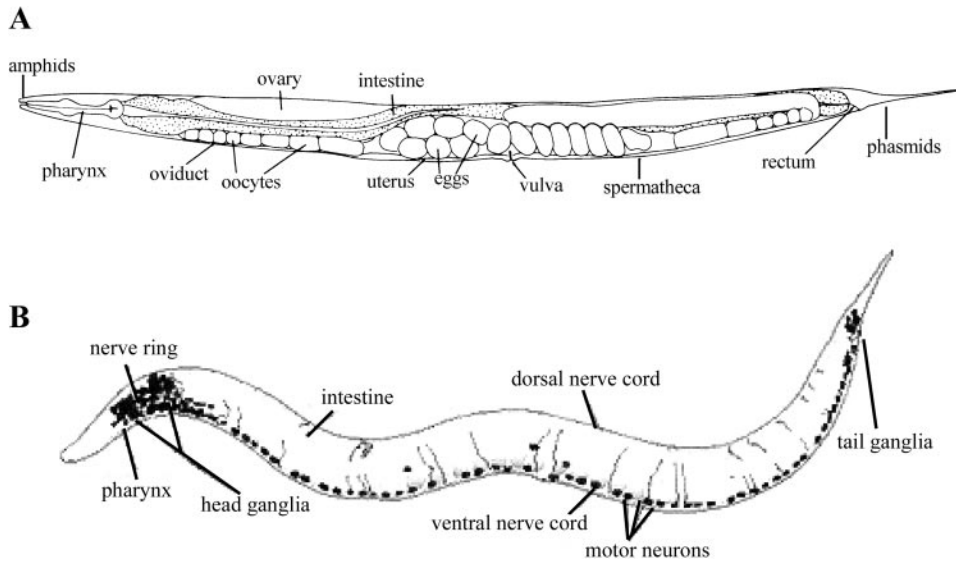
A

B

Fig. 2. *A*: schematic of the major anatomical structure of the hermaphrodite nematode. *B*: the position of the neuronal cell bodies. [Adapted, with permission, from Sulston and Horvitz (37) and courtesy of L. Salkoff.]

adults that remain separate from the main body syncytium (29, 42). Seam cells secrete collagens to form the extracellular cuticle of the nematode. Seam cells are also responsible for the shrinkage that occurs during the dauer molt (28), a process of facultative diapause that follows pheromonal or environmental cues (9, 10). Mutations in cuticle collagen genes and the process of dauer formation can cause changes in the nematode's body morphology, and disruption of *clh-1* has been shown to result in a nematode with increased body width (29). This suggests that CLH-1 may be important for certain seam cell functions. In addition to seam cells, we found that *clh-1*::GFP drove expression in both neurons and hypodermal cells in the head of the nematode, in the D-cells of the vulva, which connect the uterus to the body syncytium, and in posterior cells of the intestine (Fig. 3, *A–D*). In addition, in late larval and adult stages, as the worm reached sexual maturity, a fluorescence signal was detected in the spermatheca (Fig. 3*A*). As hermaphrodites, nematodes are able to fertilize their own eggs. The spermatheca, which lies between the oviduct and the uterus, is the site of fertilization. Finally, in recently hatched L1 larvae, expression appeared to be limited to seam cells, seen as rows of 10 blast cells that run along each lateral line, and the head neurons (Fig. 3, *E* and *F*). Some autofluorescence is detectable in the gut of these and other transgenic animals, which is mainly due to ingested bacteria.

A *clh-2b* promoter element directed expression to body wall muscle, which occurs in four quadrants on the dorsal and ventral sides of the animal (Fig. 4, *A* and *B*). These muscles are involved in locomotion; the backward propagation of a contractile wave along a dorsal quadrant is balanced by an antiphase wave along the opposing ventral quadrant, resulting in the sinusoidal movement characteristic of *C. elegans*. Expression from the *clh-2b* promoter was also observed in cell bodies of the head and tail ganglia (Fig. 4, *A–C*). *C. elegans* contains 302 neurons out of a total of 959 total

somatic nuclei. Of these, ~50 are involved in maintaining awareness of the environment through exposure to soluble compounds and volatile odorants (chemotaxis), heat and cold (thermotaxis), or touch avoidance (mechanosensation). The cell bodies of these neurons, as do most, map generally to either a site surrounding the pharyngeal bulb, with axons extending to the amphid sensilla near the mouth or to a region near the anus, extending processes to the phasmid sensilla in the tail (Ref. 43; see Fig. 2, *A* and *B*).

Clh-2b::GFP is also expressed in the posterior cells of the intestine, apparently coincident with expression from the *clh-1* promoter (Fig. 4*D*, compare to Fig. 3). The earliest larval expression of *clh-2* appears at the L1 stage, predominantly in the muscle and neuronal cells (Fig. 4, *G* and *H*). Although GFP expression from the *clh-2* promoter has previously been examined (31), that promoter is contained entirely within intron 1 of *clh-2b* and does not overlap the 4 kb of sequence used here, nor do the expression patterns overlap (see Table 1).

The *clh-3b* promoter caused GFP expression in the excretory cell. The excretory system consists of three cells: a large, H-shaped excretory cell, a duct cell, and a pore cell (27). The excretory cell body is situated ventrally, near the terminal bulb of the pharynx, and extends two side arms along the lateral lines. It is the largest mononucleate cell in the body and is coupled to a gland cell via desmosomes. Laser ablation studies suggest that the excretory cell is important for osmoregulation and the maintenance of internal hydrostatic pressure (28).

We also observed expression in the anterior four epithelial cells of the intestine, in enteric muscles and in select neurons, including the hermaphrodite-specific neurons, which are required for normal egg laying (Fig. 5, *A, B, E*, and *F*). This pattern corresponds well with that reported previously for *clh-3* (31), despite the use of separate, but overlapping, promoter elements. In addition, we noted expression in a structure surround-
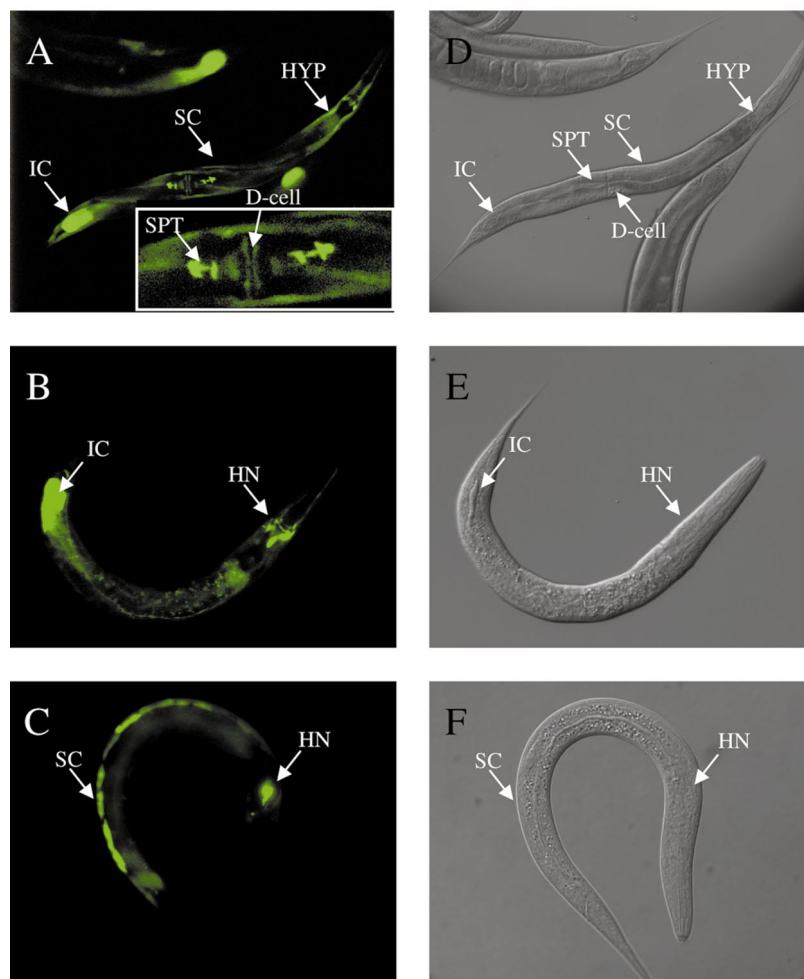
clh-1

Fig. 3. Green fluorescent protein (GFP) expression directed by the *clh-1* promoter in transgenic nematodes. Fluorescent expression patterns for nematodes expressing GFP as a transcriptional fusion from a 4-kb *clh-1* promoter (*A–C*) and the corresponding differential interference contrast (DIC) photomicrographs (*D–F*). The nematode in *A* and *D* is facing with its head upward and to the right. In this late L4/adult animal, expression is observed in the hypodermal cells of the head (HYP), unidentified cells of the spermathecal structure (SPT), seam cells (SC), the D-cell of the vulva (D-cell), and posterior intestinal cells (IC), as depicted both in the main figure and the magnified inset of the vulva area (*A*). Expression is also observed in neurons of the adult head and their associated processes (*B*) and in neurons and seam cells in a recently hatched L1 larvae, shown with its head facing down and on the right (*C*).

ing the developing embryos, which is most likely the uterus (Fig. 5, *C* and *D*). We observed this fluorescence most strongly in worms that contain only a few embryos, and the signal intensity diminished as the number of embryos increased (data not shown). We also found that the intestinal cells and tail neurons expressed GFP at the earliest larval stage (Fig. 5, *E* and *F*).

As reported previously for *clh-4* (31), the *clh-4b* promoter drove expression of GFP in a single cell, the H-shaped excretory cell (Fig. 6), where it overlapped with expression from the *clh-3* and *clh-5* promoters (Figs. 5 and 7; see below). The convergence of three separate CLH proteins within the excretory cell suggests that these genes may be of critical importance for normal function of this cell, i.e., osmoregulation.

A *clh-5*::GFP fusion directed expression to nearly every cell in the nematode (Fig. 7). At low magnifications, many of the transgenic nematodes from the *clh-5*::GFP lines appeared to fluoresce everywhere, making an exhaustive discrimination of specific structures unrealistic, as shown (Fig. 7*A*). For orientation purposes, we have indicated in Fig. 7*A* several of the

most prominent features observed in this transgenic strain. By examining mosaic animals, however, which have lost the injected array from cells of specific lineages (see DISCUSSION), we were able to more carefully delineate specific areas of expression. We show here that the excretory cell and overlying seam cells express GFP (Fig. 7*C*), as do the body wall muscles and ventral and dorsal nerve cords (Fig. 7*D*). Fluorescence was seen in neurons both in the head and tail (Fig. 7, *F* and *H*), as well as in their associated processes. We also observed expression in gut and distal tip cells, as well as in germ line cells in the ovaries of F1 and F2 generation transgenic animals (data not shown). Although we have not documented here every cell in which we observe GFP expression, these results indicate that *clh-5* expression may be ubiquitous.

The *clh-6* promoter directed expression of GFP to a wide variety of cells as well (Fig. 8). We observed intestinal fluorescence, predominantly in the most anterior and posterior segments (Fig. 8*A*), as shown for *clh-1* (Fig. 3), *clh-3b* (Fig. 5), and *clh-5* (Fig. 7). The coincidence of these four isoforms in various cells of the intestine suggests an important role for chloride flux in this organ.
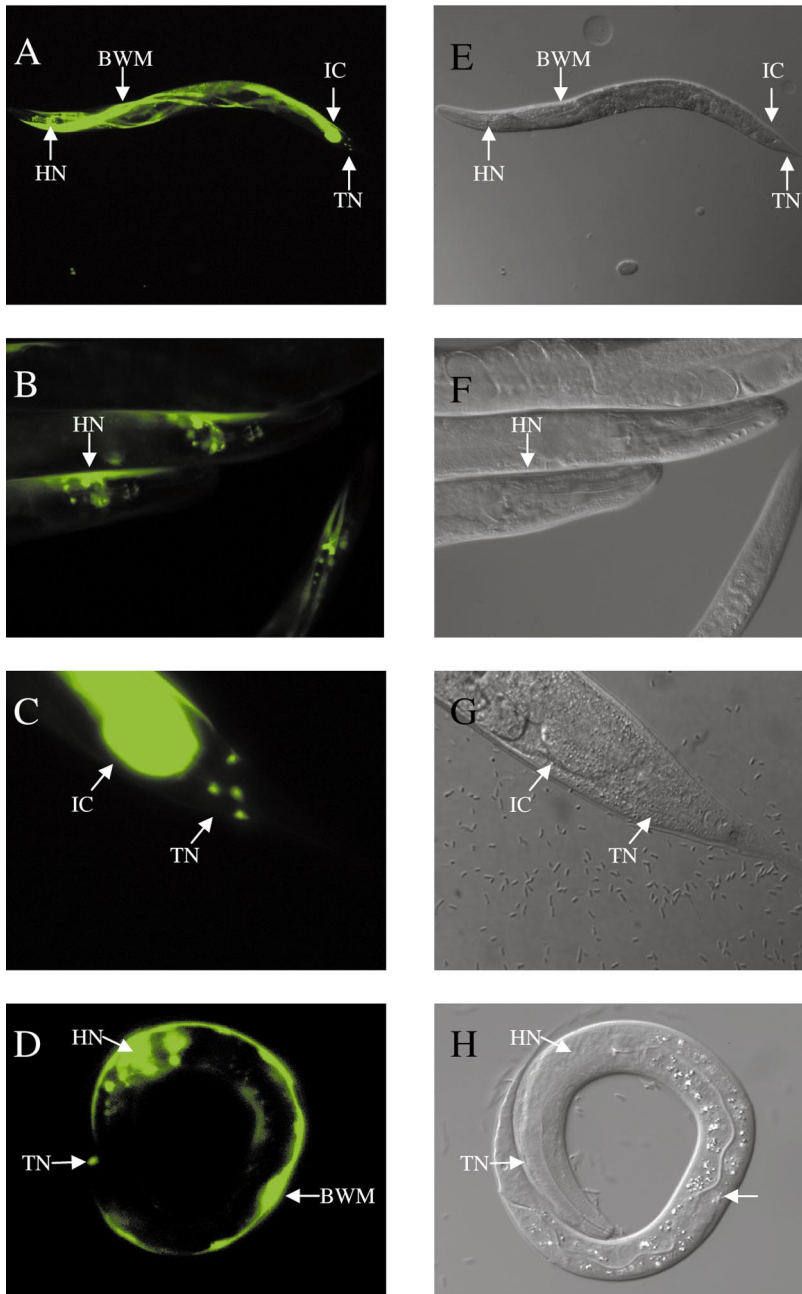
clh-2b

Fig. 4. GFP expression directed by the *clh-2b* promoter in transgenic nematodes. Fluorescent expression patterns for nematodes expressing GFP as a transcriptional fusion from a 4-kb *clh-2b* promoter (*A–D*) and the corresponding DIC photomicrographs (*E–H*). Expression is observed in the adult body wall muscle (BWM), posterior IC, tail neurons (TN), and head neurons (HN) of the nematode lying with its head to the left in *A*. Higher magnification images of fluorescent adult head and tail neurons are shown in *B* and *C*, respectively. *D*: a recently hatched L1 larvae (head facing down and coiled inside) expressing GFP in body wall muscles as well as head and tail neurons. Whether these neurons are the same as those in which the *clh-2* promoter directs expression in the adult is unknown.

The main body of the intestine in *C. elegans* consists of a tube of 20 cells, each bearing a dense layer of microvilli on their apical surface. The primary function of the intestine is probably to secrete digestive enzymes into the lumen and to absorb the processed nutrients. The intestine can serve as one of the primary storage points for protein, carbohydrate, and lipid granules in the body, as well as yolk proteins, and plays a major role in the nurture of germ cells (18).

Fluorescence also occurred in nearly all of the muscle cells, including body wall (Fig. 8*C*), vulval (Fig. 8*D*), pharyngeal (Fig. 8*B*), and excretory muscles, such as the anal depressor muscle depicted in Fig. 8*E*. In the *C.*

elegans hermaphrodite, the expulsion step of defecation depends on the coordinated contraction of three enteric muscle groups: the anal depressor muscle, the intestinal muscles, and the sphincter muscle. These muscles are activated by excitatory GABA neurotransmission (25) and receive synaptic input only from the DVB ring interneuron (43). We did not, however, observe strong fluorescence from the *clh-6* promoter in any neurons, which differs from most of the other family members except the excretory cell-specific *clh-4*.

Functional expression of clh chloride channels in Sf9 cells. We infected Sf9 cells with viruses encoding the putative *C. elegans* chloride channels. Of the five pu-
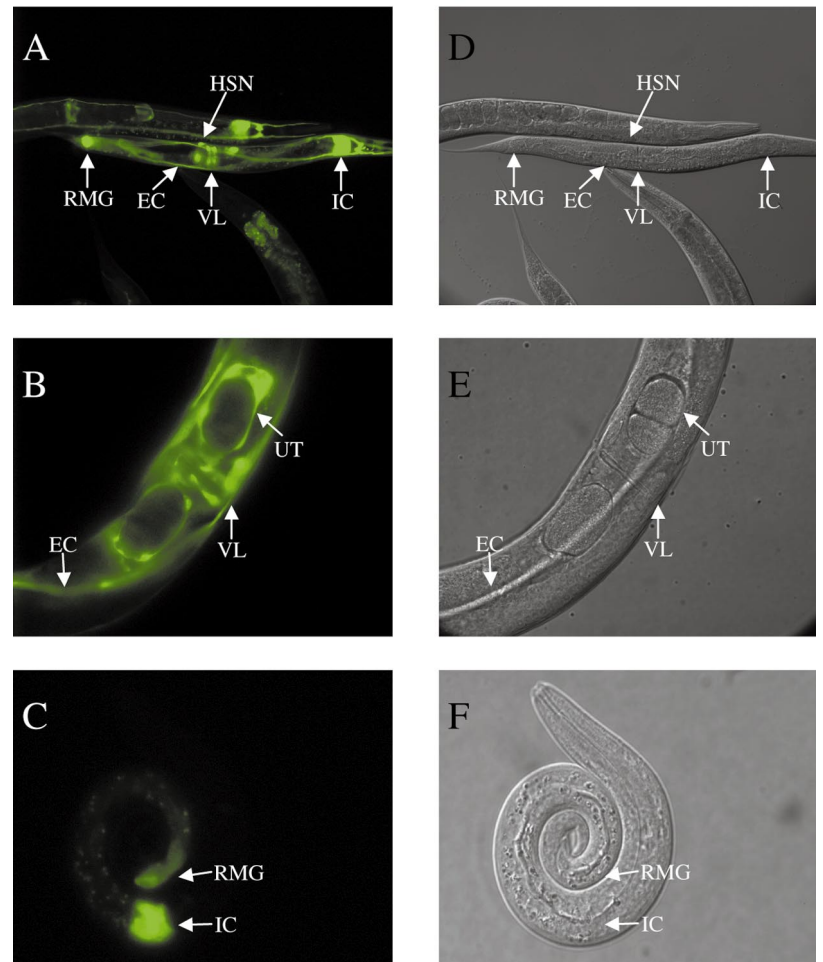
clh-3b

Fig. 5. Expression pattern of a *clh-3*::GFP promoter fusion in transgenic nematodes. Fluorescent (*A–C*) and DIC photomicrographs (*D–E*) illustrate expression of GFP from a 4-kb fragment of the *clh-3b* promoter in the following cells: anterior intestinal epithelial cells (IC), vulval cells (VL), the excretory cell (EC), the hermaphrodite-specific neuron (HSN), and rectal muscles (RMG) of the late L4/adult facing right in *A*; VL, uterine cells (UT), and EC of the adult in *B*; and RMG and anterior IC of the L1 larvae facing with its head up in *C*.

tative channels that we infected, two expressed robust time- and voltage-dependent currents in Sf9 cells. Examples of currents from cells infected with virus coding for CLH-1 and CLH-3b channels are shown in Fig. 9. The *inset* in Fig. 9*A* contains currents from cells infected with CLH-1 virus in response to 80-ms voltage pulses to −120, −80, and −40 mV. There was very little current at −40 mV, but fast-activating currents were activated at more negative potentials. The steady-state currents at the indicated potentials are illustrated (closed squares) in the main part of Fig. 9*A*.

Sf9 cells infected with wild-type virus expressed currents that were always <0.1 nA and showed no significant rectification. An example of these currents is included (open circles) in Fig. 9*A*.

Examples of currents from cells infected with virus coding for CLH-3b channels are shown in Fig. 9*B*. The *inset* contains currents in response to 500-ms voltage pulses to −120, −80, and −40 mV. CLH-3b channel currents activated more slowly (note time scale differences) and at slightly less negative potentials than CLH-1 channels, as indicated by the measurable cur-
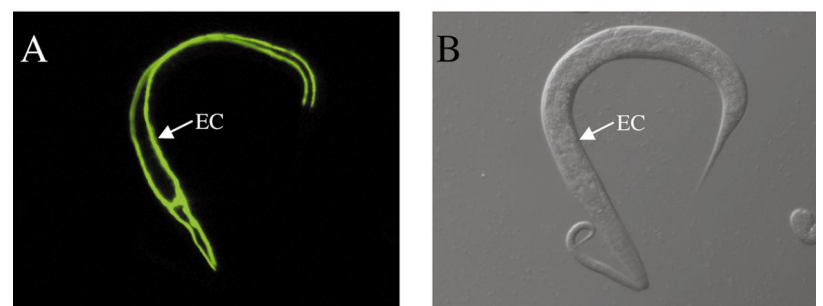
clh-4b

Fig. 6. Expression of GFP from the *clh-4b* promoter is restricted to a single cell. A 4-kb fragment of the *clh-4b* promoter drives strong GFP expression in the excretory cell, an H-shaped canal-containing cell that runs the length of the nematode and underlies the seam cells, as shown by fluorescent (*A*) and DIC (*B*) photomicrographs. The cell body of the excretory cell is positioned anterior, ventral to the terminal bulb of the pharynx.
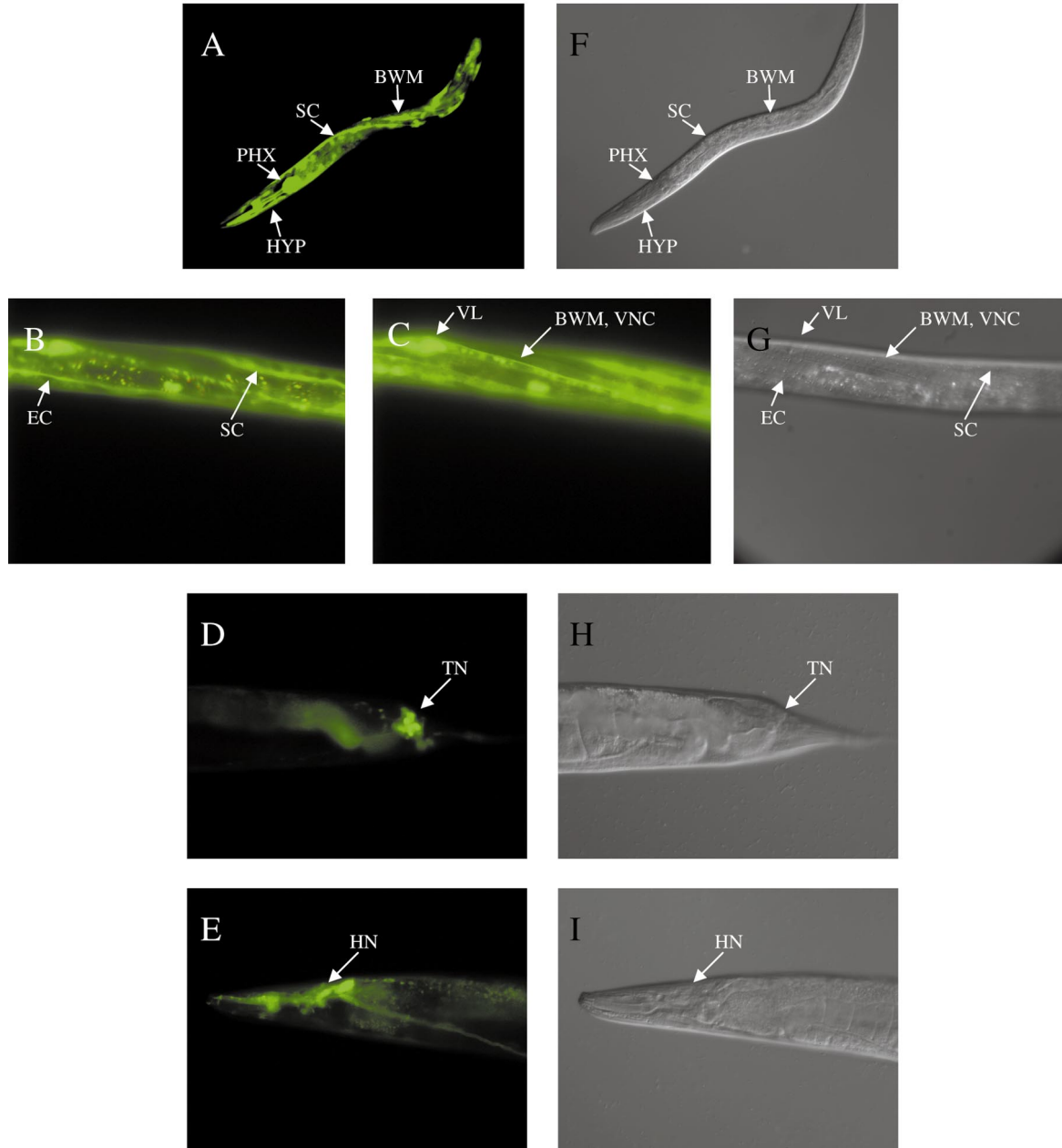
clh-5

Fig. 7. Ubiquitous expression of GFP from the *clh-5* promoter transgene illustrated by fluorescent (*A–E*) and DIC photomicrographs (*F–I*). Animals harboring a 4-kb *clh-5*::GFP promoter fragment construct expressed GFP in nearly all of the cells of the body, as shown in *A*. Although specific expression occurs in the PHX, hypodermal and muscle cells of the head (HYP), seam cells (SC), and body wall muscle (BWM), the overall high levels of fluorescence necessitate the presentation of individual organs and cells via the analysis of mosaic animals. *B* and *C* more closely examine two planes of focus in a single mosaic animal to demonstrate that the excretory cell (EC) and seam cells (SC), the vulva (VL), the ventral nerve cord (VNC), and the BWM all express some level of GFP. The bright spots in *B* arise from autofluorescent bacteria in the gut. Mosaic animals expressing GFP in cells of neuronal lineage in the tail (TN) and head (HN) are depicted in *D* and *E*, respectively. In addition, we observed GFP expression in germ line cells of the ovaries during the F1 and F2 generations of the transgenic animal (data not shown).

rent at −40 mV. The steady-state currents at the indicated potentials are illustrated (closed squares) in the main part of Fig. 9*B*.

To quantitatively assess the kinetics of the chloride channels expressed in Sf9 cells, we fit a single exponential time function to the currents in response to a voltage step to −120 mV. An example of this procedure for the CLH-1 channel currents is shown in the inset of Fig. 10. The currents (closed circles) are well described by this simple function (solid line) with a time constant of 1.25 ms. The average time constant for CLH-1 currents at this potential was 1.3 ± 0.16 ms (SE, $n = 3$).
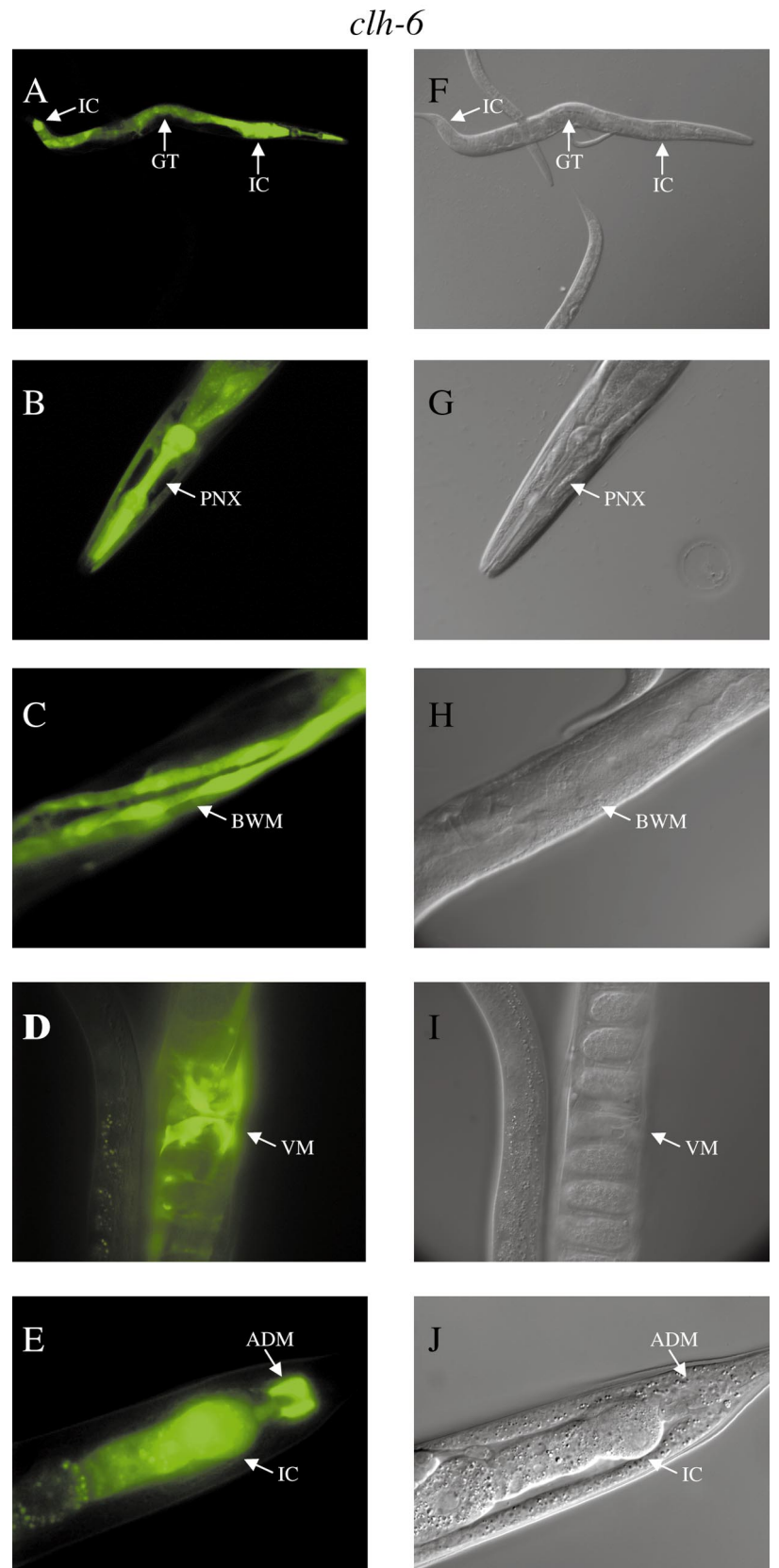
clh-6

Fig. 8. The *clh-6* promoter drives GFP expression in many of the muscle cells of the nematode. As with the *clh-5* promoter, expression of GFP by the 4-kb *clh-6* promoter resulted in highly fluorescent animals, as well as a high level of mosaicism. Therefore, the fluorescent (*A–E*) and corresponding DIC (*F–J*) photomicrographs were drawn from representative animals where GFP is expressed in only a subset of the cells normally visualized. Several of those cells are shown, as follows. *A*: the gut (GT) and anterior and posterior intestinal cells (IC) are fluorescent; *B*: the pharnyx (PNX) expresses GFP; *C*: body wall muscles (BWM) are labeled; *D*: vulval muscles (VM) fluoresce, as do the anal depressor muscle (ADM) and IC in *E*. We do not observe either seam cells or excretory cell expression. However, several neurons can be visualized under GFP optics, but expression levels are small compared with the nonneuronal cells.
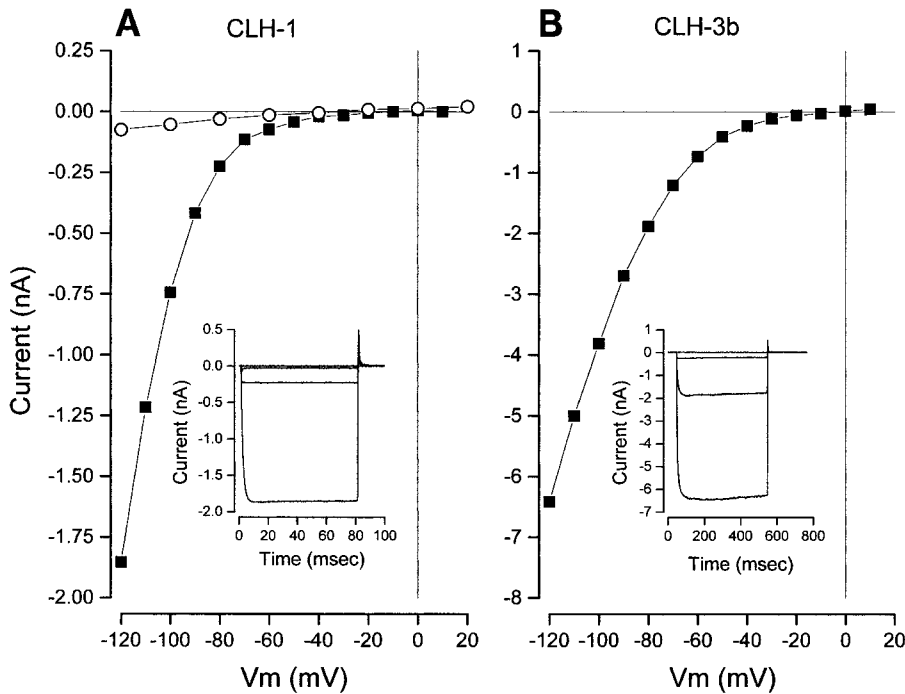
Fig. 9. Expression of *C. elegans* chloride channels. *A, inset*: currents from Sf9 cells infected with virus coding for CLH-1 in response to 80-ms depolarizations to -120, -80, and -40 mV (largest to smallest) from a holding potential of 0 mV. *A*, main figure: currents (■) from an Sf9 cell infected with virus coding for CLH-1 measured at the end of the 80-ms pulses at the indicated membrane voltages and currents (○) from a cell infected with wild-type virus. *B, inset*: currents from Sf9 cells infected with virus coding for CLH-3b in response to 500-ms depolarizations to -120, -80, and -40 mV (largest to smallest) from a holding potential of 0 mV. *B*, main figure: currents measured at the end of the 500-ms pulses at the indicated membrane voltages.

CLH-3b channels activated almost sixfold slower with an average time constant at -120 mV of 7.4 ± 0.68 ms ($n = 3$). The kinetics of ClC2 channels expressed in Sf9 cells were somewhat variable but were considerably slower than those through CLH-1 or CLH-3b channels with a mean time constant of 270 ± 69 ms ($n = 3$).

We estimated the voltage sensitivity of expressed channel activation by an analysis of the channel conductance (see EXPERIMENTAL PROCEDURES). The voltage dependence of CLH-1 channel conductance is illustrated in the main part of Fig. 10 (closed squares). These data were fit with the Boltzmann relation (*Eq. 2* and solid line in Fig. 10). From similar fits to the conductances of CLH-1, CLH-3b, and ClC2 channels, the midpoint of channel activation ($V_{1/2}$) was determined, and these are listed in Table 2. Of the three channels, ClC2 had the most positive $V_{1/2}$ value. The value for CLH-3b channels was somewhat more negative, but this difference was not significant. CLH-1 channels activated at significantly more negative potentials than CLH-3b and ClC2 channels with a $V_{1/2}$ value of -110 mV.

The parameter k in the Boltzmann relation (*Eq. 2*) reflects the steepness of the conductance-voltage relationship. The properties of the expressed chloride channels also differed in this parameter (Table 2). CLH-3b and ClC2 channels had a similar voltage sensitivity, but CLH-1 channels had a substantially greater sensitivity.

DISCUSSION

Six voltage-activated chloride channel genes are predicted based on the sequencing of the *C. elegans* genome. cDNA sequences for five of these have been previously reported, and the respective genes have been named *clh-1* through *clh-5* (31). We have reported here the cDNA sequence of the sixth and final isoform, *clh-6*. We have also identified variants of *clh-2, clh-3,* and *clh-4*, which we have termed *clh-2b, clh-3b,* and *clh-4b*. Comparisons between these variants at the genomic structure and protein levels are summarized in Fig. 1. Alternate translation initiation or stop sites and alternate splicing appear to result in changes, for the most part, to the amino and carboxy termini of the proteins. We have also confirmed the genomic structure of *clh-5* and defined the organization of the *clh-6* gene.

The nematode genome appears to code for representatives from each of the three branches of the mammalian ClC family. Clustal analysis indicates that protein isoforms CLH-1 through CLH-4 are most closely related to the mammalian ClC2 family, while CLH-5 is more closely related to mammalian ClC3, ClC4, and ClC5, and CLH-6 is related to mammalian ClC6 and ClC7. The *clh-5* and *clh-6* genes contain fewer introns than *clh-1, clh-2b, clh-3b,* or *clh-4b* and both code for proteins of <800 amino acids, which is significantly smaller than the 880–1,084 amino acid length of the other isoforms. They are also expressed nearly ubiquitously, compared with the relatively restricted expression of *clh-1, clh-2, clh-3,* and *clh-4*. Despite obvious sequence similarities between *clh-1, clh-2, clh-3*, and *clh-4*, the genomic organization (Fig. 1) suggests that there is no conserved intron-exon structure within the *clh* family.

To study the normal expression pattern of each CLH protein, transgenic nematode strains were created where GFP production is driven from a *clh* promoter. Because plasmid transmission in nematodes occurs via an extrachromosomal array, a phenomenon known as
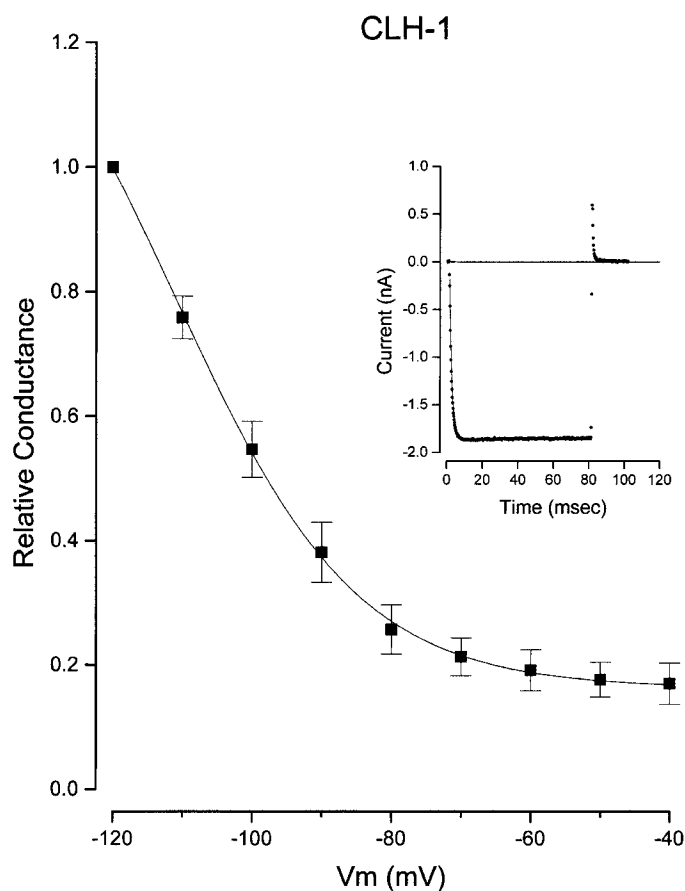
CLH-1

Fig. 10. Voltage dependence of activation of CLH-1. *Inset*: current (●) from an Sf9 cell infected with virus coding for CLH-1 in response to an 80-ms pulse to −120 mV. Line: fit of a single exponential time function to the data with a time constant of 1.25 ms. Main figure: conductance (obtained from currents measured at the end of 80-ms pulses) at the indicated membrane potentials. Mean values ($n = 3$) and SE limits. Line: fit of the Boltzmann relation (*Eq. 2*) with $V_{1/2}$ and k values of −100 ± 1.9 mV and 13 ± 0.82 mV^{-1}, respectively.

mosaicism exists (26) whereby the array becomes lost during cell division, resulting in lineage-specific deficits in expression. Mosaicism, combined with a general lack of expression of extrachromosomal arrays in germ line cells and arbitrary determination of what defines the "promoter region," combine to confound the analysis of transgenic nematodes. Expression patterns obtained from transgenes are generally acknowledged to be preliminary until confirmed via antibody staining or in situ analysis. With these caveats in mind, we have presented data generated from at least three stable lines for each *clh* promoter construct and have indicated in RESULTS which lines are mosaic.

The *clh-1*, *clh-2b*, *clh-3b*, and *clh-4b* promoters drive specific patterns of GFP expression, ranging from one to over a dozen cells labeled. In agreement with previous results (29) we have shown that the *clh-1* promoter drives expression of GFP in seam cells (Fig. 3). Tc1 transposon-mediated mutagenesis of the *clh-1* gene causes a change in body width of the adult, indicating that this protein is functionally important for the development of a normal nematode morphology (29). We

have also demonstrated *clh-1* promoter-driven expression in the D-cell of the vulva, neurons in the head of the nematode, posterior cells of the intestine, and cells of the spermathecal structure (Fig. 3; Table 1). In addition to the morphological phenotype in the Tc1 mutant, there may be unrecognized functional deficits associated with other cell types expressing CLH-1. These cells may have been missed in the earlier study due to the expression construct; the *clh-1* promoter drove expression of a nuclear-targeted β-galactosidase enzyme. Given that seam cells are multinucleate and run the length of the body, the signal arising from other cells could be masked. Alternatively, the GFP enzyme that we have used contains multiple synthetic intron sequences that can stabilize the message and result in increased protein production.

The *clh-2b* promoter demonstrated a totally different, nonoverlapping cellular expression pattern than the *clh-2* promoter (31), as summarized in Table 1. The *clh-2* promoter corresponds to sequences contained in the first intron of *clh-2b*, and, as indicated, the two promoters do not overlap. The fact that there are differences in the amino acid sequences and in the expression patterns for these *clh-2* variants suggests that the expressed proteins may have different physiological roles. However, it is difficult to assign physiological roles for these channels, since we did not observe channel activity for CLH-2b in the Sf9 cell expression system and expression of the CLH-2 protein in *Xenopus* oocytes (31) produced currents that were too small to study.

The cellular distribution patterns for the two *clh-3* variants were identical [excretory cell, intestinal cells, rectal muscles, and the hermaphrodite-specific neuron (31); Table 1], except that the *clh-3b* promoter drove expression in the uterus, as well. The predicted start site for translation of *clh-3* differs from that of *clh-3b* by almost 3 kb. Given the respective promoter fragments used for each study and their corresponding overlap, one of two possibilities exists: either 1 kb of sequence upstream of the *clh-3* start site is enough to drive the specific pattern of expression observed or the expression pattern derived from the *clh-3* promoter fragment in reality originates from the *clh-3b* start site. The mutated ATG in the *clh-3b* promoter is in frame with GFP and may give rise to a translational fusion if translation does begin upstream at the predicted start site for *clh-3*. Deletion analysis may be

Table 2. *Biophysical properties of C. elegans chloride channels*

Channel	$V_{1/2}$, mV	k, mV^{-1}	τ, ms at −120 mV
CLH-1	−110 ± 1.9	13 ± 0.82	1.3 ± 0.16
CLH-3b	−87 ± 11	29 ± 9.9	7.4 ± 0.68
mClC2	−75 ± 12	26 ± 8.1	270 ± 69

Values are means ± SE limits; $n = 3$. As described in EXPERIMENTAL PROCEDURES, we determined the midpoint ($V_{1/2}$) and the steepness (voltage sensitivity, k) of the channel conductance-voltage relation (see *Eq. 2*). Listed also is the dominant time constant for channel activation at a potential of −120 mV.

required to determine the functional boundaries of the *clh-3* promoter.

The expression driven by the promoters of both *clh-4* variants is particularly striking, because it occurs only in the excretory cell (Fig. 6 and Ref. 31). Laser ablation studies have demonstrated that the excretory cell is required for maintenance of osmotic balance and internal hydrostatic pressure in the nematode (28). Nematodes lacking an excretory cell bloat and die within 24 h, and it has been shown that the activity of the cell is responsive to changes in external osmolarity (28). The ability of the *clh-4* promoter to confine transcription to this single kidneylike cell makes it a useful tool in examining excretory cell defects using reverse genetics and antisense inhibition, especially in cases where a whole organism gene ablation may be lethal.

In contrast to the other isoforms, both *clh-5* and *clh-6* were expressed in many cells, although *clh-6* expression was limited mainly to cells of nonneuronal origin. Thus the physiological role of these ubiquitous chloride channels could reflect a function necessary for all cells.

We have functionally expressed two of the six ClC-like channels from *C. elegans*, CLH-1 and CLH-3b. Like mammalian ClC2 (38), these channels exhibit strong inward rectification. However, the amino-terminal cytoplasmic domain, which has been implicated in the gating of ClC2, is not conserved among these three proteins (13). While both CLH-1 and CLH-3b are inwardly rectifying, they activate >200- and 30-fold faster than ClC2, respectively. Moreover, CLH-1 activates at more negative voltages than ClC2 and CLH-3b. Previous attempts to functionally express CLH-1 in *Xenopus* oocytes and HEK-293 cells were unsuccessful (31). This may be due to characteristics of the expression system, because we used Sf9 cells, or to differences arising from a change in the sequence reported by others and ourselves (29) that adds 38 amino acids to the amino terminus of the protein.

CLH-3b appears to arise from a splice variant of an isoform that was recently shown to possess channel activity when expressed in *Xenopus* oocytes (31). The CLH-3 (31) and CLH-3b variants appear to generate similar current-voltage relations. The physiological role of having two variants with similar properties expressed in the same cells is unknown. Although both proteins share a common amino acid core, significant differences do occur at the amino and carboxy termini of the protein (Fig. 1*B*), suggesting some individualized function. A better understanding of those functions may first necessitate deciphering how these channels relate to the particular functions endogenous to the cells in which they are expressed.

ClC2 and ClC3 are postulated to act as volume-sensitive chloride channels, which suggests that they may be involved in cell volume regulation (41, 45). Water movement is often coupled to chloride transport, so the expression of CLH-3 channels could mediate the osmoregulatory role of the excretory cell and fluid secretion in the intestinal cells. However, it was noted that CLH-3 did not respond to cell swelling when expressed in *Xenopus* oocytes (31). We have not exam-ined the responsiveness of CLH-3b to swelling in Sf9 cells, largely due to high background currents. Voltage-gated chloride channels may also be involved directly in regulating the membrane potential or could produce changes in the chloride equilibrium potential, both of which could have secondary effects on the activity of other cell properties (33). The robust expression from the promoters for both CLH-1 and CLH-3b in neurons also suggests an important physiological role for these anion channels. However, to date, these types of channels have not been identified in *C. elegans* neuronal cells or neuromuscular junctions (11, 30). RNAi or TC1 transposon mutagenesis combined with behavioral studies may help us to reconcile these observations or uncover a role that is difficult to observe through electrophysiology.

Even in mammalian cells, the role of most ClC isoforms in basic cellular function and physiology has yet to be well defined. One of the advantages of *C. elegans* as a model system is that both genetic and reverse genetic screens are accessible. The ability to rapidly generate cell-specific antisense inhibition of a given chloride channel isoform or to employ RNAi knockdown of message levels along with the evolving techniques involved in in situ patch clamp of the worm (22) may allow us to answer very specific questions about the role of chloride channels in defined cellular events, such as transepithelial transport, neurotransmission, and muscle excitation. In addition, since a complete lineage map and fate determinations are available for every cell in *C. elegans*, this model system may be used to address the relevant question of the role of chloride channels during development. To this end, the results presented here and in previous work in this area (29, 31) provide the foundation for advancements in our understanding of both nematode biology and channel biology in general.

REFERENCES

1. **Adachi S, Uchida S, Ito H, Hata M, Hiroe M, Marumo F, and Sasaki S.** Two isoforms of a chloride channel predominantly expressed in thick ascending limb of Henle's loop and collecting ducts of rat kidney. *J Biol Chem* 269: 17677–17683, 1994.
2. **Arreola J, Melvin JE, and Begenisich T.** Volume-activated chloride channels in rat parotid acinar cells. *J Physiol (Lond)* 484: 677–687, 1995.
3. **Brandt S and Jentsch TJ.** ClC-6 and ClC-7 are two novel broadly expressed members of the CLC chloride channel family. *FEBS Lett* 377: 15–20, 1995.
4. **Caceci MS and Cacheris WP.** Fitting curves to data. *Byte* 9: 340–362, 1984.
5. **Cannon CL, Basavappa S, and Strange K.** Intracellular ionic strength regulates the volume sensitivity of a swelling-activated anion channel. *Am J Physiol Cell Physiol* 275: C416–C422, 1998.
7. **Fahlke C, Yu HT, Beck CL, Rhodes TH, and George ALJ.** Pore-forming segments in voltage-gated chloride channels. *Nature* 390: 529–532, 1997.

8. **Friedrich T, Breiderhoff T, and Jentsch TJ.** Mutational analysis demonstrates that ClC-4 and ClC-5 directly mediate plasma membrane currents. *J Biol Chem* 274: 896–902, 1999.

9. **Golden JW and Riddle DL.** The *Caenorhabditis elegans* dauer larva: developmental effects of pheromone, food, and temperature. *Dev Biol* 102: 368–378, 1984.

10. **Golden JW and Riddle DL.** A pheromone influences larval development in the nematode *Caenorhabditis elegans*. *Science* 218: 578–580, 1982.

11. **Goodman MB, Hall DH, Avery L, and Lockery SR.** Active currents regulate sensitivity and dynamic range in *C. elegans* neurons. *Neuron* 20: 763–772, 1998.

12. **Greene JR, Brown NH, DiDomenico BJ, Kaplan J, and Eide DJ.** The GEF1 gene of *Saccharomyces cerevisiae* encodes an integral membrane protein, mutations in which have effects on respiration and iron-limited growth. *Mol Gen Genet* 241: 542–553, 1993.

13. **Gründer S, Thiemann A, Pusch M, and Jentsch TJ.** Regions involved in the opening of ClC-2 chloride channel by voltage and cell volume. *Nature* 360: 759–762, 1992.

14. **Huang XY and Hirsh D.** A second trans-spliced RNA leader sequence in the nematode *Caenorhabditis elegans*. *Proc Natl Acad Sci USA* 86: 8640–8644, 1989.

15. **Jentsch TJ, Friedrich T, Schriever A, and Yamada H.** The CLC chloride channel family. *Pflügers Arch* 437: 783–795, 1999.

16. **Jentsch TJ, Steinmeyer K, and Schwarz G.** Primary structure of *Torpedo marmorata* chloride channel isolated by expression cloning in *Xenopus* oocytes. *Nature* 348: 510–514, 1990.

17. **Kawasaki M, Uchida S, Monkawa T, Miyawaki A, Mikoshiba K, Marumo F, and Sasaki S.** Cloning and expression of a protein kinase C-regulated chloride channel abundantly expressed in rat brain neuronal cells. *Neuron* 12: 597–604, 1994.

18. **Kimble J and Sharrock WJ.** Tissue-specific synthesis of yolk proteins in *Caenorhabditis elegans*. *Dev Biol* 96: 189–196, 1983.

19. **Koch MC, Steinmeyer K, Lorenz C, Ricker K, Wolf F, Otto M, Zoll B, Lehmann-Horn F, Grzeschik KH, and Jentsch TJ.** The skeletal muscle chloride channel in dominant and recessive human myotonia. *Science* 257: 797–800, 1992.

20. **Kramer JM, French RP, Park EC, and Johnson JJ.** The *Caenorhabditis elegans* rol-6 gene, which interacts with the sqt-1 collagen gene to determine organismal morphology, encodes a collagen. *Mol Cell Biol* 10: 2081–2089, 1990.

21. **Lloyd SE, Pearce SH, Fisher SE, Steinmeyer K, Schwappach B, Scheinman SJ, Harding B, Bolino A, Devoto M, Goodyer P, Rigden SP, Wrong O, Jentsch TJ, Craig IW, and Thakker RV.** A common molecular basis for three inherited kidney stone diseases. *Nature* 379: 445–449, 1996.

22. **Lockery SR and Goodman MB.** Tight-seal whole-cell patch clamping of *Caenorhabditis elegans* neurons. *Methods Enzymol* 293: 201–217, 1998.

23. **Maduke M, Pheasant DJ, and Miller C.** High-level expression, functional reconstitution, and quaternary structure of a prokaryotic ClC-type chloride channel. *J Gen Physiol* 114: 713–722, 1999.

24. **Matsumura Y, Uchida S, Kondo Y, Miyazaki H, Ko SB, Hayama A, Morimoto T, Liu W, Arisawa M, Sasaki S, and Marumo F.** Overt nephrogenic diabetes insipidus in mice lacking the CLC-K1 chloride channel. *Nat Genet* 21: 95–98, 1999.

25. **McIntire SL, Jorgensen E, Kaplan J, and Horvitz HR.** The GABAergic nervous system of *Caenorhabditis elegans*. *Nature* 364: 337–341, 1993.

26. **Mello CC, Kramer JM, Stinchcomb D, and Ambros V.** Efficient gene transfer in *C. elegans*: extrachromosomal maintenance and integration of transforming sequences. *EMBO J* 10: 3959–3970, 1991.

27. **Nelson FK, Albert PS, and Riddle DL.** Fine structure of the *Caenorhabditis elegans* secretory-excretory system. *J Ultrastruct Res* 82: 156–171, 1983.

28. **Nelson FK and Riddle DL.** Functional study of the *Caenorhabditis elegans* secretory-excretory system using laser microsurgery. *J Exp Zool* 231: 45–56, 1984.

29. **Petalcorin MI, Oka T, Koga M, Ogura K, Wada Y, Ohshima Y, and Futai M.** Disruption of clh-1, a chloride channel gene, results in a wider body of *Caenorhabditis elegans*. *J Mol Biol* 294: 347–355, 1999.

30. **Richmond JE and Jorgensen EM.** One GABA and two acetylcholine receptors function at the *C. elegans* neuromuscular junction. *Nat Neurosci* 2: 791–797, 1999.

31. **Schriever AM, Friedrich T, Pusch M, and Jentsch TJ.** CLC chloride channels in *Caenorhabditis elegans*. *J Biol Chem* 274: 34238–34244, 1999.

32. **Simon DB, Bindra RS, Mansfield TA, Nelson-Williams C, Mendonca E, Stone R, Schurman S, Nayir A, Alpay H, Bakkaloglu A, Rodriguez-Soriano J, Morales JM, Sanjad SA, Taylor CM, Pilz D, Brem A, Trachtman H, Griswold W, Richard GA, John E, and Lifton RP.** Mutations in the chloride channel gene, *CLCNKB*, cause Bartter's syndrome type III. *Nat Genet* 17: 171–178, 1997.

33. **Staley K, Smith R, Schaack J, Wilcox C, and Jentsch TJ.** Alteration of GABAA receptor function following gene transfer of the CLC-2 chloride channel. *Neuron* 17: 543–551, 1996.

34. **Steinmeyer K, Klocke R, Ortland C, Gronemeier M, Jockusch H, Gründer S, and Jentsch TJ.** Inactivation of muscle chloride channel by transposon insertion in myotonic mice. *Nature* 354: 304–308, 1991.

35. **Steinmeyer K, Ortland C, and Jentsch TJ.** Primary structure and functional expression of a developmentally regulated skeletal muscle chloride channel. *Nature* 354: 301–304, 1991.

36. **Steinmeyer K, Schwappach B, Bens M, Vandewalle A, and Jentsch TJ.** Cloning and functional expression of rat CLC-5, a chloride channel related to kidney disease. *J Biol Chem* 270: 31172–31177, 1995.

37. **Sulston JE and Horvitz HR.** Post-embryonic cell lineages of the nematode, *Caenorhabditis elegans*. *Dev Biol* 56: 110–156, 1977.

38. **Thiemann A, Gründer S, Pusch M, and Jentsch TJ.** A chloride channel widely expressed in epithelial and non-epithelial cells. *Nature* 356: 57–60, 1992.

38a.**Thompson JD, Higgins DG, and Gibson TJ.** CLUSTRAL W: improving the sensitivity of progressive multiple sequence alignment through sequence weighting, position-specific gap penalties and weight matrix choice. *Nucleic Acids Res* 22: 4673–4680, 1994.

39. **Uchida S, Sasaki S, Furukawa T, Hiraoka M, Imai T, Hirata Y, and Marumo F.** Molecular cloning of a chloride channel that is regulated by dehydration and expressed predominantly in kidney medulla. *J Biol Chem* 268: 3821–3824, 1993. [Corrigenda. *J Biol Chem* 269: July 1994, p. 19192.]

40. **Van Doren K and Hirsh D.** Trans-spliced leader RNA exists as small nuclear ribonucleoprotein particles in *Caenorhabditis elegans*. *Nature* 335: 556–559, 1988.

41. **Wang L, Chen L, and Jacob TJ.** The role of ClC-3 in volume-activated chloride currents and volume regulation in bovine epithelial cells demonstrated by antisense inhibition. *J Physiol (Lond)* 524: 63–75, 2000.

42. **White J.** The anatomy. In: *The Nematode Caenorhabditis elegans*, edited by Wood WB. Cold Spring Harbor, NY: Cold Spring Harbor, 1988, p. 81–122.

43. **White JG, Southgate E, Thompson JN, and Brenner S.** The structure of the nervous system of *Caenorhabditis elegans*. *Philos Trans R Soc Lond B Biol Sci* 314: 1–340, 1986.

44. **Wood WB** (Editor). *The Nematode Caenorhabditis Elegans*. Cold Spring Harbor, NY: Cold Spring Harbor, 1988.

45. **Xiong H, Li C, Garami E, Wang Y, Ramjeesingh M, Galley K, and Bear CE.** ClC-2 activation modulates regulatory volume decrease. *J Membr Biol* 167: 215–221, 1999.